$^{10}B(^{7}Li,^{7}Be)^{10}Be$ charge-exchange reaction

A. Etchegoyen, M. C. Etchegoyen, E. D. Izquierdo, D. Abriola, D. E. Di Gregorio, J. O. Fernández Niello, A. M. J. Ferrero, S. Gil, A. O. Macchiavelli, A. J. Pacheco, and J. E. Testoni
Departamento de Física, Comisión Nacional de Energía Atómica, 1429 Buenos Aires, Argentina
(Received 16 February 1988)

The $^{10}B(^{7}Li,^{7}Be)^{10}Be$ charge-exchange reaction has been measured at $E_{lab}=39$ MeV. Calculations were performed using a microscopic distorted-wave Born approximation with both central and tensor forces with an optical model potential obtained by fitting measured elastic scattering data. Several residual two-body interactions were used for which the absolute cross-section magnitudes varied at most within factors of two. The calculations showed that the one-step mechanism is very important for this particular reaction even at this low bombarding energy.

I. INTRODUCTION

Charge-exchange measurements have been very useful both in reaction mechanism studies and in elucidating aspects of nuclear forces. In this paper we present a study of the charge-exchange reaction $^{10}B(^{7}Li,^{7}Be)^{10}Be$ at $E_{lab}=39$ MeV. There are several previous studies[1-5] for the ($^{7}Li,^{7}Be$) charge-exchange probe on a variety of targets: ^{16}O, ^{26}Mg, ^{28}Si, and ^{40}Ca. The present reaction on ^{10}B has some specific characteristics which are worth mentioning. The reaction Q value (-1.42 MeV) is close to the optimum Q value ($\simeq 0.2$ MeV, see Sec. III A). Other reaction mechanisms, aside from the one-step mode, appear to be of lesser significance, in particular the sequential transfer process for which important routes (2^+ excited states in ^{8}Be) are blocked by isospin-mixing effects for all ^{10}Be final states. Other reaction processes that could be involved in the present charge-exchange reaction are compound nucleus and triton transfer [i.e., $^{10}B(^{7}Li,^{10}Be)^{7}Be$, $Q_{opt}\simeq 8.5$ MeV]. Further information on this will be provided in the text.

In Sec. II of this paper the experimental method is presented while in Sec. III, the work related to the microscopic one-step direct charge-exchange model is detailed. In this latter section a quick assessment of a possible sequential process is performed. After that, we review the partial wave decomposition of the form factor in the microscopic theory, making comments on some specific methods of the coordinate representation. Then, the numerical calculations are presented and a comparison of the microscopic distorted-wave Born approximation (DWBA) to the experimental data is performed. Four two-body residual interactions were tested in an effort to study the uncertainties that might arise from the previously mentioned interactions. These forces were: (i) the $M3Y$ interaction[6] derived from the Reid potential even components plus the odd state matrix elements of Elliott, (ii) an interaction, to be called $R3Y$,[6] derived from a Reid potential that has no odd components, (iii) an $M3Y$ interaction plus a pseudopotential as introduced by Petrovich *et al.*[7,8] and, finally, (iv) the potential suggested by Hosaka, Kubo, and Toki (HKT).[9]

II. EXPERIMENTAL METHOD

Beams of ^{7}Li at 39 MeV were obtained from the 20UD tandem accelerator at Buenos Aires. The beam was focused to produce a spot 1 mm wide at the target. The target was a 97.2% enriched 98 $\mu g/cm^2$ ^{10}B foil with a 30 $\mu g/cm^2$ ^{12}C backing. The presence of oxygen and carbon in the target foil does not interfere with the charge-exchange reaction of interest since the corresponding reactions have a much more negative Q value. The reaction products were detected in a telescope consisting of two surface barrier detectors, the acceptance angle being set by a collimator 1.5 mm wide, 12 mm high located 150 mm from the target. Absolute cross sections were computed by measuring the integrated beam charge. The yield of the elastically scattered ions was continuously monitored with a detector fixed at 20°. Conventional electronics were used to process the ΔE-E signals and a particle identification box was used to discard elastic events. Data were recorded in an event-by-event mode in order to perform off-line analyses. The final particle identification was obtained from the range-energy law[10] and the ^{7}Be yield was clearly separated since the ^{8}Be particle unstable ejectiles do not reach the telescope.

Rutherford scattering measurements of ^{7}Li from a 1.33 mg/cm^2 ^{197}Au target were intercalated between long charge-exchange runs in order to check the energy calibration and the absolute cross-section normalizations. The error in the absolute cross section was estimated to be less than 20%.

An energy spectrum for the $^{10}B(^{7}Li,^{7}Be)^{10}Be$ reaction is shown in Fig. 1. The energy resolution was 150 keV, which is sufficient to resolve $^{7}Be(\frac{3}{2}^-$, g.s.) from $^{7}Be(\frac{1}{2}^-$, 0.43 MeV): each of the doublets shown in the previously mentioned figure corresponds to a given state of ^{10}Be and either the ground state or the first excited state of ^{7}Be. Therefore the three doublets labeled in Fig. 1 correspond to $^{10}Be(0^+$, g.s.), $^{10}Be(2^+$, 3.37 MeV) and $^{10}Be(2^+$, 5.96 MeV) with either $^{7}Be(\frac{3}{2}^-$, g.s.) or $^{7}Be(\frac{1}{2}^-$, 0.43 MeV). It should be mentioned that the third doublet might have contributions from other peaks (for which theoretical angular distributions have not been calculated in the present analysis): $^{10}Be(1^-$, 5.96 MeV), $^{10}Be(0^+$, 6.18

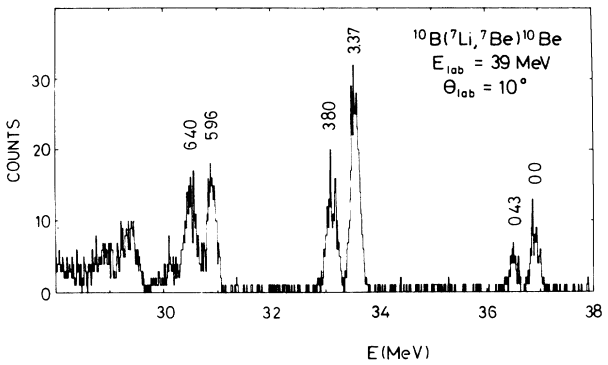

FIG. 1. Experimental spectrum of ^{7}Be ejectiles for the ^{10}B(^{7}Li,^{7}Be)^{10}Be reaction at $\theta_{lab}=10°$.

MeV), and ^{10}Be(2^-, 6.26 MeV). There is a quite small contribution that prevents the 5.96 MeV peak from being clearly separated from the 6.40 MeV peak as in the other two doublets.

III. THE CHARGE-EXCHANGE REACTION

The charge-exchange reaction ^{10}B(^{7}Li,^{7}Be)^{10}Be has been analyzed within the framework of the microscopic one-step direct charge-exchange model neglecting recoil effects and including both central and tensor forces. In order to perform the numerical calculations a computer code has been written. This computer code uses the one-body transition densities produced by a standard shell-model code, OXBASH,[11] in order to obtain the $C^{ls_0J}_{\rho_i\rho_j}$ coefficients defined in Eq. (11) of Sec. III B. Once the form-factor calculation is finished the distorted-wave Born approximation computer program MARS (Ref. 12) is called. The bound-state wave functions were generated by varying the depth of a Woods-Saxon potential so as to bind the particle at the correct binding energy while the optical potential parameters were obtained from a fit to the elastic scattering data as mentioned in Sec. III B.

Other reaction processes that could be involved in the present charge-exchange reaction are compound nucleus, triton transfer [i.e., ^{10}B(^{7}Li,^{10}Be)^{7}Be, $Q_{opt}\simeq 8.5$ MeV] and sequential transfer. The compound-nucleus process has already been analyzed[5] at $E_{lab}=24$ MeV using a Hauser-Feshbach formalism and it was concluded that the compound nucleus does not contribute to any appreciable extent. The triton reaction channel has been considered in this work since both the ^{7}Be ejectiles from the charge-exchange mode and the ^{7}Be residual nucleus from the triton transfer are detected and added to the same experimental peak. The triton transfer to the ground-state peak was studied in the present work by generating SU(3) triton wave functions in the p shell with $(\lambda,\mu)=(3,0)$ in order to obtain the relevant shell-model parentage amplitudes. The calculated cross section was several orders of magnitude below the experimental data and presented a different shape for the angular distribution. A quick assessment of a possible sequential process will now be performed for ^{10}B(^{7}Li,^{7}Be($\frac{3}{2}^-$, g.s.)^{10}Be(0^+,g.s.).

A. Sequential transfer assessment

Considering for the first and second step of the sequential mode only one-particle transfers, it can be seen that the only intermediate route nuclei are ^{6}Li+^{11}B or ^{8}Be+^{9}Be. Assuming that the states of interest are well described by p-shell wave functions, the "intermediate targets" (i.e., the intermediate heavy nuclei ^{11}B or ^{9}Be) must have spin $\frac{3}{2}$ so as to couple the 3^+ in ^{10}B to the 0^+ in ^{10}Be.

Preliminary coupled-reaction-channel calculations performed with the computer code SESIME (Ref. 13) showed that the most important intermediate routes to the ^{7}Be($\frac{3}{2}^-$,g.s.)+^{10}Be(0^+,g.s.) seem to be through ^{9}Be($\frac{3}{2}^-$)+^{8}Be(2^+). The ^{9}Be($\frac{3}{2}^-$) ground state carries almost all the single-particle strength[14] and therefore it is the only one to be considered as "intermediate target." On the other hand, there are three ^{8}Be(2^+) states with any significant p-shell single-particle strength:[14] the 2.94, 16.63, and 16.92 MeV states. It is remembered that although in the present section only the reaction leading to ^{10}Be(0^+,g.s.) is studied, the previously mentioned three ^{8}Be(2^+) states would be important for any final ^{10}Be states due to their large spectroscopic amplitudes.

The kinematic selectivity for this charge-exchange (cx) reaction gives an optimum Q value close to zero [$Q^{cx}_{opt}\simeq(Z_eZ_r-Z_pZ_t)e^2/R$, where the Z_i are the charges of the projectile, target, ejectile, and residual nuclei and R is the sum of the projectile and target radii], irrespective of the reaction mechanism. If there were a further kinematic-matching condition for the sequential mode, i.e., an optimum excitation energy in the intermediate ^{8}Be(2^+)+^{9}Be($\frac{3}{2}^-$) channel, this energy would be close to 11 MeV.[15] As was already mentioned, there are three ^{8}Be(2^+) states with significant p-shell single-particle strength: the 2.94, 16.63, and 16.92 MeV states, the last two states lying closer to 11 MeV. Nevertheless, these two better-matched states cannot be intermediate routes as it will now be shown.

These two states are the isospin-mixed 2^+ states and they have been extensively studied.[16,17] Had they had a unique isospin they would have had an admixture of ^{7}Be($\frac{3}{2}^-$,g.s.)+n and ^{7}Li($\frac{3}{2}^-$,g.s.)+p configurations. It is most interesting that this is not the case but, on the contrary, the 16.63 MeV state has a ^{7}Li($\frac{3}{2}^-$,g.s.)+p configuration while the 16.92 MeV state has a ^{7}Be($\frac{3}{2}^-$,g.s.)+n configuration.[16,17] Therefore, even though the spectroscopic factors for these levels (assuming no isospin mixing) are large they cannot be intermediate routes for a ^{7}Li($\frac{3}{2}^-$,g.s.)$\rightarrow{}^{8}$Be$\rightarrow{}^{7}$Be($\frac{3}{2}^-$,g.s.) sequential process owing to their single-particle nature: the first step would only populate the 16.63 MeV ^{7}Li($\frac{3}{2}^-$,g.s.)+p state whereas the second step can only proceed via the 16.92 MeV ^{7}Be($\frac{3}{2}^-$,g.s.)+n state and therefore these states are blocked by isospin-mixing effects. These remarks can be extended to ^{7}Be($\frac{1}{2}^-$,0.43 MeV) as a final state. As already mentioned the first step can only

proceed via ^{8}Be(2^+,16.63 MeV) and therefore ^{8}Be(2^+,16.92 MeV) is blocked. In order to prove that the other 2^+ state is also blocked for a ^{7}Li($\frac{3}{2}^-$,g.s.) $\rightarrow{}^8$Be$\rightarrow{}^7$Be($\frac{1}{2}^-$,0.43 MeV) route we need to show that ^{8}Be(2^+,16.63 MeV) has no ^{7}Be($\frac{1}{2}^-$,0.43 MeV)$+n$ strength. The ^{8}Be(2^+,16.63 MeV) isospin-mixed wave function[17] can be written as

$$|\,^8\mathrm{Be}(2^+,16.63\ \mathrm{MeV})\rangle = 0.74\,|\,J=2^+,T=0\rangle + 0.67\,|\,J=2^+,T=1\rangle\ .$$

The isospin-dependent parentage amplitude is

$$S(j,t_z)=CS_T(j)=\langle\, T'T'_z\tfrac{1}{2}t_z \mid TT_z\,\rangle \frac{\langle JT|||a^\dagger_{j1/2}|||J'T'\rangle}{[(2J+1)(2T+1)]^{1/2}}\ ,$$

where J',T' are ^{7}Be quantum numbers and j,t_z are transferred-particle quantum numbers. After replacing the ^{8}Be(2^+,16.63 MeV) wave function for a $p_{3/2}$ transfer we obtain

$$S(\tfrac{3}{2},\tfrac{1}{2})=\langle\, \tfrac{1}{2}-\tfrac{1}{2}\tfrac{1}{2}\tfrac{1}{2} \mid 00\,\rangle S_{T=0}(\tfrac{3}{2}) + \langle\, \tfrac{1}{2}-\tfrac{1}{2}\tfrac{1}{2}\tfrac{1}{2} \mid 10\,\rangle S_{T=1}(\tfrac{3}{2})\ .$$

The parentage amplitudes $S_T(\frac{3}{2})$ obtained with the (6–16)2B interaction of Ref. 18 are

$$S_{T=0}(\tfrac{3}{2})=0.51 \quad \text{and} \quad S_{T=1}(\tfrac{3}{2})=0.43$$

and therefore the spectroscopic factor is

$$S^2(\tfrac{3}{2},\tfrac{1}{2})=0.003$$

which is negligible.

As a final word, it is remembered that in this section we only showed that the sequential process is hindered but it has not been proven that it is of no importance for the present charge-exchange reaction. A more satisfying way of assessing the relative importance of this mode is to perform reliable coupled-reaction-channel calculations.

B. Microscopic form factor for the one-step direct charge exchange

The one-step contribution has been analyzed within the framework of the microscopic one-step direct charge-exchange model including both central and tensor forces. Details on the partial-wave decomposition in the coordinate representation for a central force can be found in Ref. 19 and in the present section an extension to tensor forces will be highlighted. Studies of the use of the momentum representation for microscopic folded form factors are shown in Refs. 3 and 20. The most general form factor for an $A(a,b)B$ reaction may be given as:

$$F(\mathbf{R})=\langle\, I_BM_BT_BM_{TB};s_bm_bt_bm_{tb} \mid \sum_{t,p} V_{t,p} \mid s_am_at_am_{ta};I_AM_AT_AM_{TA}\,\rangle\ , \tag{1}$$

where I_i and s_i are the angular momenta, T_i and t_i are the isospins for the nucleus "i." The nucleus-nucleus interaction may be written as

$$V_{t,p}=V(\mathbf{r}_{t,p})=\sum_{\substack{s_0,t_0\\K=0,2}} V^K_{s_0t_0}(r_{t,p})C^K_{s_0}\sum_{\substack{\nu,\nu'\\M,n_0}}(-)^{M+n_0}\langle\, s_0s_0\nu\nu' \mid KM\,\rangle\sigma^{s_0}_\nu(p)\sigma^{s_0}_{\nu'}(t)\tau^{t_0}_{n_0}(p)\tau^{t_0}_{-n_0}(t)Y_{K,-M}(\hat{r}_{t,p})\ . \tag{2}$$

Here $\mathbf{r}_{t,p}$ is the spatial coordinate between the interacting target nucleon "t" and the interacting projectile nucleon "p" and $\mathbf{R}$ is the channel radius as displayed in Fig. 2; $K=0$ corresponds to the central force and $K=2$ to the tensor force. The operators σ^{s_0} and τ^{t_0} are the spin and isospin Pauli operators, respectively, when $s_0=t_0=1$ whereas they become the unit operators when $s_0=t_0=0$. The constants $C^K_{s_0}$ have the values $C^0_0=\sqrt{4\pi}$, $C^0_1=-\sqrt{12\pi}$, and $C^2_1=\sqrt{24\pi/5}$. Following Ref. 12 we define $F^{JSL_{\rm tr}}_{M_{\rm tr}}(\mathbf{R})$ through the expression

$$F(\mathbf{R})=\sqrt{4\pi}\sum_{\substack{JSL_{\rm tr}\\M_{\rm tr}}} i^{-L_{\rm tr}}h(\,ABab,JSL_{\rm tr})F^{JSL_{\rm tr}}_{M_{\rm tr}}(\mathbf{R}) \tag{3}$$

with

$$h(\,ABab,JSL_{\rm tr})=(-)^{I_A-M_A+s_b-m_b+S+M_S}\langle\, I_AM_AI_B-M_B \mid JM_J\,\rangle\langle\, s_am_as_b-m_b \mid SM_s\,\rangle\langle\, JM_JSM_S \mid L_{\rm tr}-M_{\rm tr}\,\rangle\ , \tag{4}$$

where, $J(S)$ is the total spin transferred to the intrinsic motion of the target (projectile) system, $L_{\rm tr}$ is the angular-

momentum transferred, $I_{A(B)}$ is the total spin of $A(B)$, $s_{a(b)}$ is the total spin of $a(b)$. $F^{JSL_{\rm tr}}_{M_{\rm tr}}(\mathbf{R})$ in the coordinate system shown in Fig. 2 is

$$F^{JSL_{\rm tr}}_{M_{\rm tr}}(\mathbf{R})=\sum_{\substack{l_1,l_2,L_{12}\\ Ks_0t_0n_0}} d^{JSL_{\rm tr}}_{l_1l_2L_{12};Ks_0t_0n_0} f^{JSL_{\rm tr},M_{\rm tr}}_{l_1l_2L_{12};Ks_0t_0}(\mathbf{R}) , \tag{5}$$

where l_1 and l_2 are the angular-momenta transferred to the intrinsic motion of the target and projectile systems, respectively, and they couple to L_{12}. Also

$$d^{JSL_{\rm tr}}_{l_1l_2L_{12};Ks_0t_0n_0}=(4\pi)^{-1/2}i^{L_{\rm tr}-(l_1+l_2)}(-)^{s_a-s_b+S+n_0}C^{K}_{s_0} \times\hat{s}_b\hat{I}_B\hat{L}_{12}\hat{K}\begin{Bmatrix} S & J & L_{\rm tr}\\ l_2 & l_1 & L_{12}\\ s_0 & s_0 & K\end{Bmatrix}\langle T_BT_{Bz}\,|\,T_AT_{Az}t_0-n_0\rangle\langle t_bt_{bz}\,|\,t_at_{az}t_0n_0\rangle , \tag{6}$$

and

$$f^{JSL_{\rm tr},M_{\rm tr}}_{l_1l_2L_{12};Ks_0t_0}(\mathbf{R})=\int\int V^{K}_{s_0t_0}(r_{t,p})g^{l_1s_0Jt_0}_{AB}(r_1)g^{l_2s_0St_0}_{ab}(r_2)\{[Y^*_{l_2}(\hat{r}_2)Y^*_{l_1}(\hat{r}_1)]^{L_{12}}Y^*_K(\hat{r}_{t,p})\}^{L_{\rm tr}}d\mathbf{r}_1d\mathbf{r}_2 , \tag{7}$$

where $\mathbf{r}_1$ and $\mathbf{r}_2$ are the coordinates for the interacting nucleons in the target and projectile, respectively. The radial transition densities for the target and projectile system have the form

$$g^{l_1s_0Jt_0}_{AB}(r_1)=\langle I_BT_B\|\sum_t\frac{\delta(r_1-r_t)}{r_t^2}T^{l_1s_0J}(t)\tau^{t_0}(t)\|I_AT_A\rangle , \tag{8}$$

$$g^{l_2s_0St_0}_{ab}(r_2)=\langle s_bt_b\|\sum_p\frac{\delta(r_2-r_p)}{r_p^2}T^{l_2s_0S}(p)\tau^{t_0}(p)\|s_at_a\rangle , \tag{9}$$

where the tensors T^{LSJ} are defined by

$$T^{LSJ}_{M_J}=\sum_{MM_s} i^LY_{LM}\sigma^S_{M_S}\langle LMSM_S\,|\,JM_J\rangle . \tag{10}$$

The expansion of these radial transition densities in terms of one-body transition densities can be found in Ref. 21 where they are shown to give

$$g^{l_1s_0Jt_0}_{AB}(r_1)=\sum_{\rho_i\rho_j}C^{l_1s_0J}_{\rho_i\rho_j}(ABt_0)\Phi^B_{n_il_iJ_i}(r_1)\Phi^A_{n_jl_jJ_j}(r_1) , \tag{11}$$

where

$$C^{l_1s_0J}_{\rho_i\rho_j}=\sqrt{6(2J_i+1)}\langle l_iJ_i\|T^{l_1s_0J}\|l_jJ_j\rangle\mathrm{OBTD}(AB\rho_i\rho_j;Jt_0) \tag{12}$$

with the one-body transition densities (OBTD) defined by

$$\mathrm{OBTD}(AB\rho_i\rho_j;Jt_0)=\frac{\langle I_BT_B\|\{a^\dagger_{\rho_i}\tilde{a}_{\rho_j}\}^{Jt_0}\|I_AT_A\rangle}{\hat{J}\hat{t}_0} . \tag{13}$$

In Eq. (11) the sum runs over all possible single-particle states $\rho_k=|\,n_kl_kj_kt_{zk}\rangle$, $\Phi(r_1)$ are the radial wave functions for the initial and final nuclei, and the coefficients $C^{l_1s_0J}_{\rho_i\rho_j}$ are obtained from shell-model calculations. The expression for the lighter system transition density matrix is similar to Eq. (11).

Following Ref. 19 we introduce the new coordinates $\mathbf{r}_1$ and $\mathbf{r}=\mathbf{r}_2-\mathbf{r}_1$. Here we would like to draw the attention to the appearance of $Y^*_{KM}(\hat{r}_{t,p})$ in Eq. (7) arising from the tensor force. It is customary to expand spherical harmonics using a Moshinsky transformation,[22] but expansions including the radial dependence have also been proposed.[23] We propose the expansion

$$V^{K}_{s_0t_0}(r_{t,p})Y^*_{KM}(\hat{r}_{t,p})=\sqrt{\pi}\sum_{\substack{NN'\\ M_NM_{N'}}}\langle NM_NKM\,|\,N'M_{N'}\rangle Y_{NM_N}(\hat{r})Y^*_{N'M_{N'}}(\hat{R})\sum_{\varepsilon\varepsilon'\mu}D^{N'}_{N\varepsilon\varepsilon'\mu K}r^{\varepsilon}R^{\varepsilon'}X^{\mu}_K(r,R) , \tag{14}$$

with

$$D^{N'}_{N\varepsilon\varepsilon'\mu K}=\delta_{\varepsilon+\varepsilon',K}\left[\frac{(2K+1)!}{(2\varepsilon+1)!(2\varepsilon'+1)!}\right]^{1/2}\frac{\hat{\mu}\hat{K}\hat{\varepsilon}\hat{\varepsilon}'\hat{N}}{\hat{N}'}\langle N0\varepsilon0\,|\,\mu0\rangle\langle\varepsilon'0\mu0\,|\,N'0\rangle W(N\varepsilon N'\varepsilon';\mu K)\ , \tag{15}$$

with X^{μ}_{K} given by the potential inversion

$$X^{\mu}_{K}(r,R)=\int\frac{V^{K}_{s_0t_0}(\,|\,\mathbf{r}+\mathbf{R}\,|\,)}{|\,\mathbf{r}+\mathbf{R}\,|^{K}}P_{\mu}(\cos\theta)d(\cos\theta)\ . \tag{16}$$

After these preliminaries, the folding integral of Eq. (7) can be given as

$$f^{SL_{\rm tr}M_{\rm tr}}_{l_1l_2L_{12};Ks_0t_0}(\mathbf{R})=Y^{*}_{L_{\rm tr}M_{\rm tr}}(R)\sum_{\lambda\lambda'k}a_{l_1l_2L_{12}\lambda\lambda'k}I^{JSL_{\rm tr}}_{l_1l_2L_{12}\lambda\lambda'k;Ks_0t_0}(R)\ , \tag{17}$$

where

$$a_{l_1l_2L_{12}\lambda\lambda'k}=\pi\delta_{\lambda+\lambda',l_2}\left[\frac{(2l_2+1)!}{(2\lambda+1)!(2\lambda'+1)!}\right]^{1/2}\frac{\hat{l}_1\hat{l}_2\hat{\lambda}\hat{\lambda}'\hat{k}}{\hat{L}_{12}}\langle l_10\lambda0\,|\,k0\rangle\langle k0\lambda'0\,|\,L_{12}0\rangle W(l_1\lambda L_{12}\lambda';kl_2)\ , \tag{18}$$

and

$$I^{JSL_{\rm tr}}_{l_1l_2L_{12}\lambda\lambda'k;Ks_0t_0}(R)=\int dr\,r^{\lambda'+2}\sum_{\varepsilon\varepsilon'\mu}D^{L_{\rm tr}}_{L_{12}\varepsilon\varepsilon'\mu K}r^{\varepsilon}R^{\varepsilon'}X^{\mu}_{K}(r,R)\int dr_1r_1^{\lambda+2}\hat{g}^{k}_{ab}(r,r_1)g^{l_1s_0Jt_0}_{AB}(r_1)\ , \tag{19}$$

where $\hat{g}^{k}_{ab}$ is obtained by inverting $g^{l_2s_0St_0}_{ab}(r_2)$,

$$\hat{g}^{k}_{ab}(r,r_1)=\int\frac{g^{l_2s_0St_0}_{ab}(\,|\,\mathbf{r}+\mathbf{r}_1\,|\,)}{|\,\mathbf{r}+\mathbf{r}_1\,|^{l_2}}\times P_k(\cos\theta)d(\cos\theta)\ . \tag{20}$$

By comparison of Eq. (17) with the analogous one restricted to only central forces [take $K=0$ in Eq. (17) or see, for instance, Ref. 19] we see that $\mathbb{V}^{L_{\rm tr}}_{L_{12}K}(r,R)$ defined as

$$\mathbb{V}^{L_{\rm tr}}_{L_{12}K}(r,R)=\sum_{\varepsilon'\varepsilon\mu}D^{L_{\rm tr}}_{L_{12}\varepsilon\varepsilon'\mu K}r^{\varepsilon}R^{\varepsilon'}X^{\mu}_{K}(r,R) \tag{21}$$

plays the role of a generalized potential inversion.

The equations shown in this section have been coded in a computer program. As a check, several previous theoretical predictions have been recalculated. The present code gives exactly the same results (within the resolution of the drawing) of the seven angular distributions for ^{28}Si(^{7}Li,^{7}Be$_0$)^{28}Al(2$^+$,0.031 MeV) plotted in Fig. 3 of Ref. 1 whereas it predicts differences in cross-section magnitudes ranging from 0.7 to 2, approximately from those of Ref. 4. This discrepancy with Ref. 4 is to be expected since Dodd *et al.* reproduce results from Cook *et al.*[3] who predict cross sections 4π times smaller than Williams-Norton *et al.*[2] A further test was performed against the computer code of Ref. 19 which was written in the coordinate representation instead of the momentum representation as the previously mentioned codes: the ^{28}Si(^{18}O,^{18}F)^{28}Al(3$^+$,g.s.) and the ^{28}Si(^{18}O,^{18}F)^{28}Al(2$^+$,0.031 MeV) angular distributions were reproduced again within the resolution of Fig. 6 of Ref. 19.

C. One-step charge-exchange numerical calculations

In order to obtain optical-potential parameters to generate distorted waves, the elastic scattering of ^{7}Li from ^{10}B was measured at $E_{\rm lab}=39$ MeV. An optical-potential search was performed and the fit of the calculation to the experimental data is presented in Fig. 3. The parameters obtained were $V=69.7$ MeV, $a=0.97$ fm, $r_0=0.75$ fm, $W_{\rm SD}=16.8$ MeV, $a_{\rm SD}=0.68$ fm, $r_{\rm SD}=0.84$ fm, and $r_c=1.24$ fm, where the radius parameters r_0, $r_{\rm SD}$, and r_c

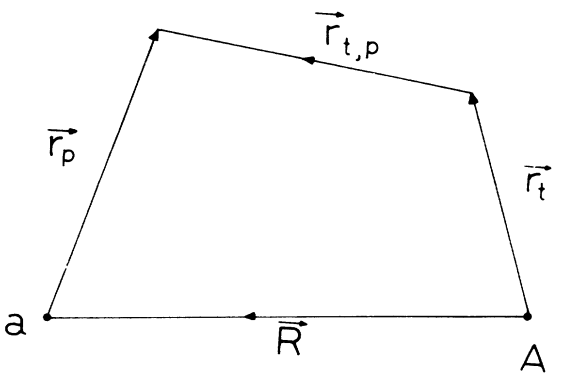

FIG. 2. Coordinate system for the microscopic direct charge-exchange form factor.

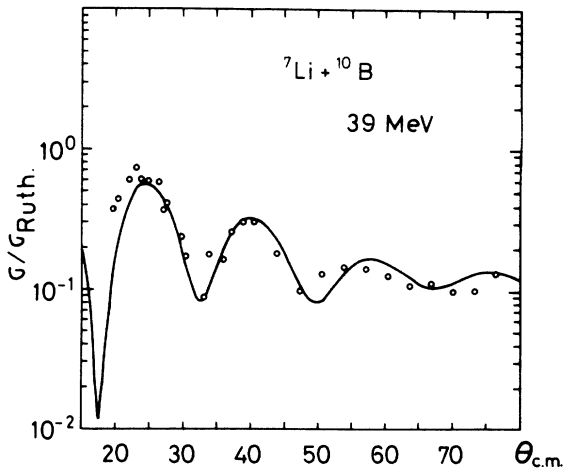

FIG. 3. Optical model fit to the ^{7}Li+^{10}B elastic reaction at 39 MeV.

follow the heavy-ion convention. Subscript SD indicates a surface-derivative imaginary potential. This potential was used for both entrance and exit channels.

In order to assess the dependence of the charge-exchange theoretical angular distributions on the optical potentials, a second parameter set was extracted from the elastic scattering data. This new potential search was performed with both a volume and a surface-derivative

TABLE I. Structure coefficients used for spin-dependent forces. Where I is equal to J (S), the spin transferred to the heavier (lighter) system and $l<,l>$ are the possible values of the angular momentum transferred to the heavier (l_1) or lighter (l_2) system. The l value of the initial states (IS) and of the final states (FS) is always 1.

IS J_i	FS J_j	I	Transfer $l<$	$l>$	OBTD	$C^{l<1I}_{\rho_i\rho_j}$	$C^{l>1I}_{\rho_i\rho_j}$
			Lighter system				
			^{7}Li($\frac{3}{2}^-$,g.s.)→^{7}Be($\frac{3}{2}^-$,g.s.)				
$\frac{1}{2}$	$\frac{1}{2}$	1	0	2	0.093	−0.052	0.148
$\frac{1}{2}$	$\frac{3}{2}$	1	0	2	−0.121	−0.194	−0.069
$\frac{3}{2}$	$\frac{1}{2}$	1	0	2	0.121	−0.194	−0.069
$\frac{3}{2}$	$\frac{3}{2}$	1	0	2	−0.102	−0.183	0.052
$\frac{1}{2}$	$\frac{3}{2}$	2	2		−0.099	−0.168	
$\frac{3}{2}$	$\frac{1}{2}$	2	2		0.099	0.168	
$\frac{3}{2}$	$\frac{3}{2}$	3	2		−0.223	−0.632	
			^{7}Li($\frac{3}{2}^-$,g.s.)→^{7}Be($\frac{1}{2}^-$,0.43 MeV)				
$\frac{1}{2}$	$\frac{1}{2}$	1	0	2	0.061	−0.035	0.098
$\frac{1}{2}$	$\frac{3}{2}$	1	0	2	0.234	0.374	0.132
$\frac{3}{2}$	$\frac{1}{2}$	1	0	2	−0.073	0.117	0.041
$\frac{3}{2}$	$\frac{3}{2}$	1	0	2	0.192	0.342	−0.097
$\frac{1}{2}$	$\frac{3}{2}$	2	2		−0.076	0.129	
$\frac{3}{2}$	$\frac{1}{2}$	2	2		0.202	0.342	
			Heavier system				
			^{10}B(3^+,g.s.)→^{10}Be(0^+,g.s.)				
$\frac{3}{2}$	$\frac{3}{2}$	3	2		0.342	0.970	
			^{10}B(3^+,g.s.)→^{10}Be(2^+,3.37 MeV)				
$\frac{1}{2}$	$\frac{1}{2}$	1	0	2	0.003	−0.002	0.005
$\frac{1}{2}$	$\frac{3}{2}$	1	0	2	0.072	0.116	0.041
$\frac{3}{2}$	$\frac{1}{2}$	1	0	2	−0.057	0.091	0.032
$\frac{3}{2}$	$\frac{3}{2}$	1	0	2	−0.059	−0.105	0.030
$\frac{1}{2}$	$\frac{3}{2}$	2	2		0.062	0.105	
$\frac{3}{2}$	$\frac{1}{2}$	2	2		−0.049	−0.083	
$\frac{3}{2}$	$\frac{3}{2}$	2	2		0.158	0.0	
$\frac{3}{2}$	$\frac{3}{2}$	3	2		−0.228	−0.646	
			^{10}B(3^+,g.s.)→^{10}Be(2^+,5.96 MeV)				
$\frac{1}{2}$	$\frac{1}{2}$	1	0	2	0.018	−0.010	0.030
$\frac{1}{2}$	$\frac{3}{2}$	1	0	2	−0.262	−0.419	−0.148
$\frac{3}{2}$	$\frac{1}{2}$	1	0	2	0.021	−0.034	−0.012
$\frac{3}{2}$	$\frac{3}{2}$	1	0	2	−0.062	−0.110	0.031
$\frac{1}{2}$	$\frac{3}{2}$	2	2		−0.084	−0.143	
$\frac{3}{2}$	$\frac{1}{2}$	2	2		−0.028	−0.048	
$\frac{3}{2}$	$\frac{3}{2}$	2	2		−0.029	0.0	
$\frac{3}{2}$	$\frac{3}{2}$	3	2		−0.065	−0.184	

imaginary parts of the type suggested in Ref. 24. The dependence was found to be unimportant.

The radial wave functions of the bound states were generated from a Woods-Saxon potential with geometrical parameters $r_0=r_c=1.25$ fm, $a_0=a_{s_0}=0.65$ fm, and $V_{s_0}=7$ MeV. Form factors were calculated with the already mentioned $M3Y$ effective interaction[6] plus a pseudopotential, i.e.,

$$V_{01}^{0}(r)=-4885.5\frac{e^{-4r}}{4r}+1175.5\frac{e^{-2.5r}}{2.5r}+310\delta(r)\ ,$$

$$V_{11}^{0}(r)=-421.3\frac{e^{-4r}}{4r}+480.0\frac{e^{-2.5r}}{2.5r}+3.5\frac{e^{-0.707r}}{0.707r}-145\delta(r)\ ,$$

$$V_{11}^{2}(r)=385.7r\frac{e^{-2.5r}}{2.5}+10.5r\frac{e^{-1.429r}}{1.429}\ ,$$

where $V_{s_0t_0}^{K}(r)$ is defined in Eq. (2). The δ forces added to the central components are an approximation to the single-nucleon knockon exchange (SNKE).[2]

The nuclear structure information, i.e., the one-body transition densities (OBTD), was obtained from the shell model using the (6–16)2B interaction of Ref. 18. These and the coefficients $C_{\rho_i\rho_j}^{ls_0J}$ as defined in Eq. (11) are shown in Tables I and II.

The ^{10}B[^{7}Li,^{7}Be($\frac{3}{2}^-$)]^{10}Be(0^+,g.s.) reaction can evolve through three different spins transferred to the lighter system, i.e., $S=1,2,3$. For $S=2$ the radial transition density as defined in Eq. (11) is

$$g_{ab}^{2121}(r_2)=-0.168\Phi_{1p1/2}^{^6\mathrm{Li}+p}(r_2)\Phi_{1p3/2}^{^6\mathrm{Li}+n}(r_2)+0.168\Phi_{1p3/2}^{^6\mathrm{Li}+p}(r_2)\Phi_{1p1/2}^{^6\mathrm{Li}+n}(r_2)$$

since the two contributing $C_{\rho_i\rho_j}^{212}$ are equal in magnitude and opposite in sign (see Table I). This expression is not identically zero owing to the dependence of the radial wave functions on either the single-particle states involved (spin-orbit partners $1p\frac{3}{2}$-$1p\frac{1}{2}$) or on the initial (or final) nucleus of the projectile system. The former dependence introduces a difference due to the spin-orbit interaction while the latter due to the Coulomb force. Since neither the spin orbit nor the Coulomb potentials play a significant role in this reactions, the $S=2$ theoretical cross section was found to be approximately 9 orders of magnitude smaller than the one-step total theoretical prediction. A supplementary calculation was performed by arbitrarily setting one of these two $C_{\rho_i\rho_j}^{212}$ to zero. The cross section did not alter the shape but it increased more than 6 orders of magnitude. We see in this limiting case the importance of the shell-model valence space and of an accurate evaluation of the transition densities.

The angular distributions for ^{7}Be($\frac{3}{2}^-$,g.s.) + ^{10}Be(0^+,g.s.) and ^{7}Be($\frac{3}{2}^-$,g.s.)+ ^{10}Be(2^+,3.37 MeV), are

TABLE II. Structure coefficients used for spin-independent force. See Table I for notation.

IS J_i	FS J_j	Transfer I	Transfer i	OBTD	$C_{\rho_i\rho_j}^{I0I}$
		Lighter system			
		^{7}Li($\frac{3}{2}^-$,g.s.)→^{7}Be($\frac{3}{2}^-$,g.s.)			
$\frac{1}{2}$	$\frac{1}{2}$	0	0	0.179	0.175
$\frac{3}{2}$	$\frac{3}{2}$	0	0	0.227	0.314
$\frac{1}{2}$	$\frac{3}{2}$	2	2	−0.099	0.137
$\frac{3}{2}$	$\frac{1}{2}$	2	2	0.099	0.137
$\frac{3}{2}$	$\frac{3}{2}$	2	2	−0.008	−0.011
		^{7}Li($\frac{3}{2}^-$,g.s.)→^{7}Be($\frac{1}{2}^-$,0.43 MeV)			
$\frac{1}{2}$	$\frac{3}{2}$	2	2	0.076	−0.106
$\frac{3}{2}$	$\frac{1}{2}$	2	2	0.202	0.279
$\frac{3}{2}$	$\frac{3}{2}$	2	2	0.173	0.240
		Heavier system			
		^{10}B(3^-,g.s.)→^{10}Be(2^+,3.37 MeV)			
$\frac{1}{2}$	$\frac{3}{2}$	2	2	0.062	−0.085
$\frac{3}{2}$	$\frac{1}{2}$	2	2	−0.049	−0.068
$\frac{3}{2}$	$\frac{3}{2}$	2	2	0.158	0.218
		^{10}B(3^-,g.s.)→^{10}Be(2^+,5.96 MeV)			
$\frac{1}{2}$	$\frac{3}{2}$	2	2	−0.084	0.116
$\frac{3}{2}$	$\frac{1}{2}$	2	2	−0.028	−0.039
$\frac{3}{2}$	$\frac{3}{2}$	2	2	−0.029	−0.040

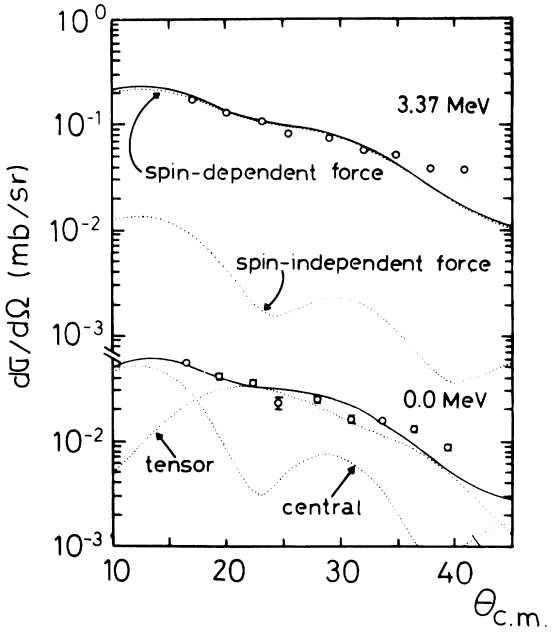

FIG. 4. Experimental and microscopic charge-exchange model cross sections for 0.0 and 3.37 MeV peaks identified in Fig. 1. Partial contributions to the theoretical angular distributions (dotted lines) as well as their sum (solid lines) are displayed. The central term includes a pseudopotential as described in the text.

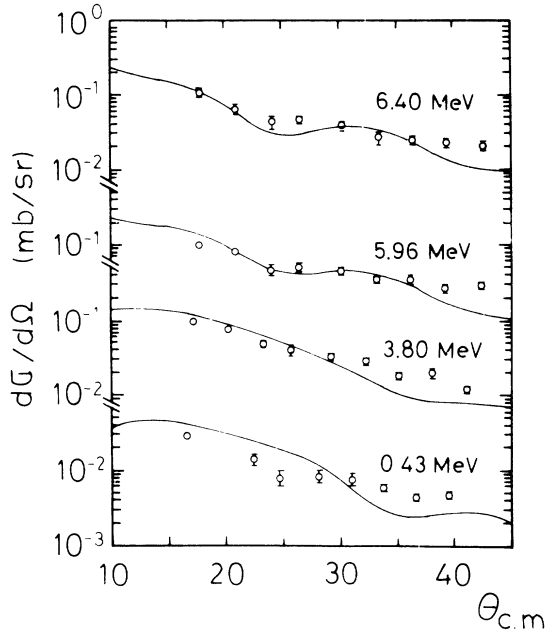

FIG. 5. Experimental and microscopic charge-exchange model angular distributions for the 0.43, 3.80, 5.96, and 6.40 MeV peaks identified in Fig. 1.

displayed in Fig. 4 while the angular distributions for the four remaining peaks identified in Fig. 1 are displayed in Fig. 5.

In Fig. 4 the partial contribution of the central and the tensor terms for the ^{10}B(0$^+$,g.s.) cross section are shown separately. The tensor term is seen to be of the same magnitude or even larger (although of a different shape) of the central term and therefore cannot be omitted as has already been suggested in Refs. 3, 4, and 6. Also, in Fig. 4, the partial contributions of the spin-dependent and spin-independent forces for the ^{10}B(2$^+$,3.37 MeV) cross section are displayed. It is observed that for the present two-body residual interaction the spin-independent force does not contribute to any appreciable extent.

The calculations seem to reproduce the measured cross sections although there is a disagreement at the most backward measured angles where all the theoretical predictions underestimate the cross sections. This might be due to several reasons, e.g., the sequential transfer mechanism.

The normalizations of the theoretical predictions to the data as used in Figs. 4 and 5 were fairly close to one and the values for the 0.0, 0.43, 3.37, 3.80, 5.96, and 6.40 MeV peaks were 0.9, 0.8, 1.3, 1.0, 1.0, and 1.4, respectively. It is seen from the previously mentioned figures that the normalizations are unambiguously determined from the data with exception of the 0.43 MeV peak. This agreement is the relevant experimental issue to support the importance of the one-step mode for the present reaction. This result should be emphasized since the current charge-exchange literature considers the one-step mechanism to be relevant at much larger bombarding energies, 30 MeV/nucleon and above (Refs. 21, 25, and references therein) whereas the two-step mechanism would dominate at lower energies. The study performed in Sec. III A was an effort in order to assess any possible contradiction with the previously mentioned results and it was argued that important intermediate routes of a possible two-step mode were blocked due to isospin mixing. Moreover, it was shown for the reaction leading to ^{10}Be(0$^+$,g.s.), that these blocked routes appear to be the most important routes.

D. Dependence of the theoretical estimates on the residual two-body interaction

Earlier charge-exchange (or inelastic) calculations would commonly use a sole central Yukawa interaction with a range of 1 fm (Ref. 26) and a review of existing data [(p,p') and (p,n) reactions] gave $V_{11}^0 = 12 \pm 2.5$ (Ref. 27) for such a force. Later on, Petrovich *et al.*[7,8] proposed to include a pseudopotential, i.e., a $\delta(\mathbf{r})$ force, in order to approximately account for the central term of the SNKE. Also, effective interactions derived by fitting matrix elements of a sum of Yukawas to G-matrix elements of phenomenological nucleon-nucleon potentials[6,9,28] were introduced. These interactions involve more than one Yukawa potential in an effort to consider different meson exchanges. The interactions used in this work as defined in the Introduction, aside from the already mentioned $M3Y$ interaction are, the $R3Y$ interaction;

TABLE III. Relative cross-section normalizations to the $M3Y$ interaction. The normalizations are defined as $\sigma_i(\theta)/\sigma_{M3Y}(\theta)$ for "i" any of the four forces.

Final state	$M3Y$	HKT	$R3Y$	$M3Y$ + delta
^{7}Li($\frac{3}{2}^-$,g.s.) + ^{10}B(3$^+$,g.s.)	1	1	0.5	0.65
^{7}Li($\frac{1}{2}^-$,0.43 MeV) + ^{10}B(3$^+$,g.s.)	1	1	0.5	0.55
^{7}Li($\frac{3}{2}^-$,g.s.) + ^{10}B(2$^+$,3.37 MeV)	1	1	0.5	0.65
^{7}Li($\frac{1}{2}^-$,0.43 MeV) + ^{10}B(2$^+$,3.37 MeV)	1	1	0.5	0.55
^{7}Li($\frac{3}{2}^-$,g.s.) + ^{10}B(2$^+$,5.96 MeV)	1	1	0.45	0.55
^{7}Li($\frac{1}{2}^-$,0.43 MeV) + ^{10}B(2$^+$,5.96 MeV)	1	1	0.45	0.55

$$V_{01}^{0}(r)=-3201.7\frac{e^{-4r}}{4r}+1001.9\frac{e^{-2.5r}}{2.5r}+1.3\frac{e^{-0.707r}}{0.707r}\ ,$$

$$V_{11}^{0}(r)=-2105.1\frac{e^{-4r}}{4r}+653.6\frac{e^{-2.5r}}{2.5r}+1.3\frac{e^{-0.707r}}{0.707r}\ ,$$

$$V_{11}^{2}(r)=314.9r\frac{e^{-2.5r}}{2.5}+7.1r\frac{e^{-1.429r}}{1.429}\ ,$$

and the HKT interaction;

$$V_{01}^{0}(r)=1109.4\frac{e^{-5r}}{5r}-8.03\frac{e^{-3r}}{3r}+123.1\frac{e^{-2r}}{2r}\ ,$$

$$V_{11}^{0}(r)=617.8\frac{e^{-5r}}{5r}-92.3\frac{e^{-3r}}{3r}+156.8\frac{e^{-2r}}{2r}+3.49\frac{e^{-0.707r}}{0.707r}\ ,$$

$$V_{11}^{2}(r)=-1121.7\ \mathrm{OBEP}(4r)+3.49\ \mathrm{OBEP}(0.707r)\ ,$$

where

$$\mathrm{OBEP}(\beta r)=\left[1+\frac{3}{\beta r}+\frac{3}{(\beta r)^2}\right].$$

The shape of the angular distributions was found to depend only mildly on the force used, which is encouraging.

The relative normalizations among the four mentioned forces for each of the six identified peaks of Fig. 1 are shown in Table III. The HKT interaction predicts the same magnitudes than the $M3Y$ interaction and they are approximately a factor of 2 larger than the $R3Y$ predictions. This suggests that the omission of the odd components needs further justification in order to discard both the $M3Y$ and HKT potentials. The HKT interaction was derived by fitting oscillator matrix elements of the G-matrix elements obtained from the Paris potential rather than from the Reid potential for the even channels and the oscillator matrix elements of Elliott for the odd channels as used for the $M3Y$ potential. Also, the HKT force has four ranges for the central components rather than three as in the $M3Y$ interaction and it has a modified functional form for the tensor components. Although the differences were many, the two forces yielded the same angular distributions for the six peaks of the present reaction. If this very preliminary conclusion were to stand further analyses, any improvements in the residual two-body force are unlikely to be made by just fitting G-matrix elements. Actually, similar conclusions were obtained from nucleon-nucleus scattering[28,29] with antisymmetrized microscopic DWBA calculations.

Finally, a comment on the calculations performed for the $M3Y$ interaction plus two pseudopotentials, viz., $3108(\mathbf{r})$ added to V_{01}^{0} and $-145\ \delta(\mathbf{r})$ to V_{11}^{0}. Golin *et al.*[7] suggested to perform an exact calculation in order to determine the zero-range strength. An exact SNKE calculation was performed for ^{10}B[^{7}Li,^{7}Be($\frac{3}{2}^{-}$,g.s.)]^{10}Be(0^{+},g.s.) and the details will be published elsewhere. The only contributing central term for the direct one-step mechanism for the ground-state peak is V_{11}^{0} since the V_{01}^{0} component cannot flip the 3^{+} state in ^{10}B to the 0^{+} state in ^{10}Be. The zero-range strength extracted from the previously mentioned calculation was 132 MeV which is in agreement with the suggested 145 MeV and therefore no ambiguities seem to arise from this model. The latter value was used for ^{40}Ca(^{7}Li,^{7}Be)^{40}K at $E_{\mathrm{lab}}=35$ MeV,[2] for ^{16}O(^{7}Li,^{7}Be)^{16}N at $E_{\mathrm{lab}}=50$ MeV,[3] and for ^{28}Si(^{7}Li,^{7}Be)^{28}Al at $E_{\mathrm{lab}}=72$ MeV, and ^{26}Mg(^{7}Li,^{7}Be)^{26}Na at $E_{\mathrm{lab}}=88$ MeV.[4]

IV. CONCLUSIONS

New experimental data for the ^{10}B(^{7}Li,^{7}Be)^{10}Be reaction have been measured and analyzed in the present work. This reaction could proceed through different mechanisms. The compound nucleus formation was studied in Ref. 5 and it was found to be unimportant. The triton transfer channel to the ground-state peak was studied in the present work and it was found to be negligible. For the sequential mechanism it was argued that important intermediate routes of a possible sequential mechanism were blocked due to isospin mixing. Moreover, it was shown for the reaction leading to ^{10}Be(0^{+},g.s.) that these blocked routes appear to be the most important routes.

Special emphasis was put on the microscopic direct one-step model including the central and the tensor components of the residual nucleon-nucleon force. An extension of the partial-wave decomposition in the coordinate representation for central forces of Ref. 19, in order to include tensor forces, has been deduced. Both types of forces, central and tensor, were important to explain the experimental data.

A study of the ambiguities arising from different residual interactions was performed and from the few cases analyzed in this work it seems that both the $M3Y$ and the HKT interactions perform equally well. The quite different G matrix approaches used to obtain the two interactions yielded, nevertheless, very similar results. The $R3Y$ interaction underpredicted the cross-section magnitudes by a factor of 2. It was also noted that the zero-range strength obtained from an exact calculation in order to account for the SNKE is quite close to the currently used value.

It is believed that the one-step process cannot be neglected for the present reaction which is an interesting issue due to the bombarding energy.

ACKNOWLEDGMENTS

We thank H. J. Maier from the University of Munich for providing the ^{10}B targets and Dr. D. Sinclair for helpful discussions. Some of us (D.E.D., J.O.F.N., A.J.P., and J.E.T.) would like to acknowledge the support of the Consejo Nacional de Investigaciones Científicas y Técnicas, Argentina.

[1]M. E. Williams-Norton, F. Petrovich, K. W. Kemper, G. M. Hudson, R. J. Puigh, and A. F. Zeller, Nucl. Phys. **A275**, 509 (1977).
[2]M. E. Williams-Norton, F. Petrovich, K. W. Kemper, R. J. Puigh, O. Stanley, and A. F. Zeller, Nucl. Phys. **A313**, 477 (1979).
[3]J. Cook, K. W. Kemper, P. V. Drumm, L. K. Fifield, M. A. C. Hotchkis, T. R. Ophel, and C. L. Woods, Phys. Rev. C **30**, 1538 (1984).
[4]A. C. Dodd, N. M. Clarke, J. Coopersmith, R. J. Griffiths, K. I. Pearce, B. Stanley, and J. Cook, J. Phys. G **11**, 1035 (1985).
[5]W. Kohler, G. Gruber, A. Steinhauser, and K. Bethge, Nucl. Phys. **A290**, 233 (1977).
[6]G. Bertsch, J. Borysowich, A. McManus, and W. G. Love, Nucl. Phys. **A284**, 399 (1977).
[7]M. Golin, F. Petrovich, and D. Robson, Phys. Lett. **64B**, 253 (1976).
[8]F. Petrovich and D. Stanley, Nucl. Phys. **A275**, 487 (1977).
[9]A. Hosaka, K. I. Kubo, and H. Toki, Nucl. Phys. **A444**, 76 (1985).
[10]N. Anyas-Weiss, J. C. Cornell, P. S. Fisher, P. N. Hudson, A. Menchaca Rocha, D. J. Millener, A. D. Panagiotou, D. K. Scott, D. Strottman, D. M. Brink, B. Buck, P. J. Ellis, and T. Engeland, Phys. Rep. C **12**, 201 (1974).
[11]A. Etchegoyen, W. D. M. Rae, and N. S. Godwin (MSU version: B. A. Brown, W. E. Ormand, and J. S. Winfield), the Oxford-Buenos Aires Shell-Model Code (unpublished).
[12]T. Tamura and K. S. Low, Comput. Phys. Commun. **8**, 349 (1974).
[13]G. Proudfoot and W. D. M. Rae, computer code SESIME (unpublished).
[14]S. Cohen and D. Kurath, Nucl. Phys. **A101**, 1 (1967).
[15]D. M. Brink, Phys. Lett. **40B**, 37 (1972).
[16]J. B. Marion, Phys. Lett. **14**, 315 (1965).
[17]F. G. Barker, Nucl. Phys. **A83**, 418 (1966).
[18]S. Cohen and D. Kurath, Nucl. Phys. **A73**, 1 (1965).
[19]B. T. Kim, A. Greiner, M. A. G. Fernandes, N. Lisbona, K. S. Low, and M. C. Mermaz, Phys. Rev. C **20**, 1396 (1979).
[20]F. Petrovich, Nucl. Phys. **A251**, 143 (1975).
[21]A. Etchegoyen, D. Sinclair, S. Liu, M. C. Etchegoyen, D. K. Scott, and D. L. Hendrie, Nucl. Phys. **A397**, 343 (1983).
[22]M. Moshinksy, Nucl. Phys. **A13**, 104 (1959).
[23]B. F. Bayman and A. Kallio, Phys. Rev. C **156**, 1121 (1967).
[24]A. J. Baltz, P. D. Bond, J. D. Garrett, and S. Kahana, Phys. Rev. C **12**, 136 (1975).
[25]J. S. Winfield, N. Anantaraman, Sam M. Austin, L. H. Harwood, J. van der Plicht, H.-L. Wu, and A. F. Zeller, Phys. Rev. C **33**, 1333 (1986).
[26]W. R. Wharton and P. T. Debevec, Phys. Rev. C **11**, 1963 (1975).
[27]S. M. Austin, *The Two-Body Force on Nuclei,* edited by S. M. Austin and G. M. Crawley (Plenum, New York, 1972).
[28]N. Anantaraman, H. Toki, and G. F. Bertsch, Nucl. Phys. **A398**, 269 (1983).
[29]M. Yabe, A. Hosaka, K. K. Kubo, and H. Toki, Prog. Theor. Phys. **73**, 1165 (1985).